Influence of Oceanic Intraseasonal Kelvin Waves on Eastern Pacific Hurricane Activity

JULIEN BOUCHAREL,[a] FEI-FEI JIN,[b,c] MATTHEW H. ENGLAND,[a] BORIS DEWITTE,[d] I. I. LIN,[e] HSIAO-CHING HUANG,[e] AND MAGDALENA A. BALMASEDA[f]

[a] *ARC Centre of Excellence for Climate System Science, University of New South Wales, Sydney, New South Wales, Australia*
[b] *Department of Atmospheric Sciences, SOEST, University of Hawai'i at Mānoa, Honolulu, Hawaii*
[c] *Laboratory for Climate Studies, Beijing Climate Center, Chinese Meteorological Agency, Beijing, China*
[d] *IRD/LEGOS/UPS, Toulouse, France*
[e] *Department of Atmospheric Sciences, National Taiwan University, Taipei, Taiwan*
[f] *European Centre for Medium-Range Weather Forecasts, Reading, United Kingdom*

(Manuscript received 3 February 2016, in final form 26 July 2016)

ABSTRACT

Recent studies have highlighted the role of subsurface ocean dynamics in modulating eastern Pacific (EPac) hurricane activity on interannual time scales. In particular, the well-known El Niño–Southern Oscillation (ENSO) recharge–discharge mechanism has been suggested to provide a good understanding of the year-to-year variability of hurricane activity in this region. This paper investigates the influence of equatorial subsurface subannual and intraseasonal oceanic variability on tropical cyclone (TC) activity in the EPac. That is to say, it examines previously unexplored time scales, shorter than interannual, in an attempt to explain the variability not related to ENSO. Using ocean reanalysis products and TC best-track archive, the role of subannual and intraseasonal equatorial Kelvin waves (EKW) in modulating hurricane intensity in the EPac is examined. It is shown first that these planetary waves have a clear control on the subannual and intraseasonal variability of thermocline depth in the EPac cyclone-active region. This is found to affect ocean subsurface temperature, which in turn fuels hurricane intensification with a marked seasonal-phase locking. This mechanism of TC fueling, which explains up to 30% of the variability of TC activity unrelated to ENSO (around 15%–20% of the total variability), is embedded in the large-scale equatorial dynamics and therefore offers some predictability with lead time up to 3–4 months at seasonal and subseasonal time scales.

1. Introduction

The eastern Pacific (EPac) is the second most active region in terms of tropical cyclone (TC) activity, and yet environmental factors regulating this activity on subseasonal to interannual time scales deserve further exploration (e.g., Dong and Holland 1994; Wang and Lee 2009; Peduzzi et al. 2012). The last two seasons (i.e., the boreal summers of 2014 and 2015) stand as the two most intense EPac hurricane seasons on record. In September 2015, an unprecedented system of three distinct category-4 hurricanes surrounded the Hawaiian archipelago, yet causing no significant damage to the region. A few weeks later, Hurricane Patricia developed rapidly into the most intense TC ever recorded, with sustained winds measured at >175 kt (1 kt $\approx 0.51\,m\,s^{-1}$) (Huang et al. 2016, manuscript submitted to *J. Geophys. Res. Oceans*). Hurricane Patricia made intense landfall along the Pacific coast of Mexico, but again spared the most populated cities in the area. However, some systems have significantly impacted this region and the U.S. Southwest (Jauregui 2003; Ritchie et al. 2011; Raga et al. 2013; Wood and Ritchie 2013). Recent evidence further suggests an increase in TC activity in the vicinity of Hawaii due to global warming (Murakami et al. 2013). In short there is renewed interest and great urgency to better understand cyclogenesis and storm intensification in the EPac region.

Supplemental information related to this paper is available at the Journals Online website: http://dx.doi.org/10.1175/JCLI-D-16-0112.s1.

Corresponding author address: Julien Boucharel, ARC Centre of Excellence for Climate System Science, University of New South Wales, Sydney, NSW 2052, Australia.
E-mail: j.boucharel@unsw.edu.au

DOI: 10.1175/JCLI-D-16-0112.1

The fundamental ENSO recharge–discharge (RD) mechanism (Jin 1997) has recently been discovered as one of the main drivers of TC intensity in the EPac (Jin et al. 2014, 2015; Boucharel et al. 2016). This mechanism operates via the meridional redistribution of ocean subsurface heat following an El Niño event toward the EPac cyclone-active region. It plays a major role during the TC season following canonical or eastern Pacific (EP) ENSO events (Rasmusson and Carpenter 1982; Harrison and Larkin 1998), such as for example the two strongest El Niños on record, 1982/83 and 1997/98, which had a strong influence in the EPac. Yet, there are other expressions of ENSO, characterized by different onset time, propagation features, or spatial structure. One particular mode of ENSO expression is the so-called central Pacific (CP) or Modoki El Niño, which exhibits a maximum anomalous warming around the international date line (Ashok et al. 2007). The influence of the RD mechanism on TC activity remains only marginal after such events, as they tend to be characterized by a meridional discharge of heat located in the center of the basin and mostly directed to the south of the equator, away from the EPac cyclone-active region (Ren and Jin 2013; Jin et al. 2015; Boucharel et al. 2016). Although all observed El Niño events have been quite different (Johnson 2013), the RD mechanism accounts overall for a significant component (≈30%) of the yearly variation of TC intensity in the EPac (Jin et al. 2014, 2015). This sheds light on the previously overlooked subsurface ocean properties and in particular the equatorial ocean dynamics as a potentially major contributor to hurricane activity in this region (Price 2009; Lin et al. 2013; Jin et al. 2014, 2015; Boucharel et al. 2016). This is further confirmed by observational and modeling studies that highlight the role of oceanic subsurface characteristics, such as thermocline depth (Balaguru et al. 2013) and stratification (Shay and Brewster 2010; Vincent et al. 2014) on TC intensification in the EPac.

The substantial progress made in ENSO theory over the past three decades (including the RD mechanism) was built upon the foundation of tropical dynamics (Neelin et al. 1998). Because of the long ocean inertia and the well-understood tropical ocean dynamics on a wide range of time scales (e.g., Kessler et al. 1995; Suarez and Schopf 1988; Battisti and Hirst 1989; Cane and Sarachik 1977; Cane et al. 1990), understanding the mechanisms of subsurface variability that affect the modulation of TC intensity can contribute toward designing more accurate hurricane forecast systems with possible longer lead time in the EPac. In particular, the linear theory of Cane and Sarachik (1977) predicts the existence of a large variety of propagative modes on a wide range of frequencies, but the EPac sea level/thermocline (and therefore subsurface temperature) variability is predominantly affected by Kelvin and Rossby waves forced by subannual (Busalacchi and O'Brien 1980, Yuan 2005) and intraseasonal (Kessler et al. 1995; Gushchina and Dewitte 2012; Mosquera-Vásquez et al. 2014) winds in the central-western Pacific (roughly 120°E–180°), in particular associated with the Madden–Julian oscillation (MJO; Madden and Julian 1994). When the basic state of the surface atmospheric circulation in the tropical Pacific (i.e., trade winds blowing from east to west) is disrupted, the deep warm water layer piled up in the western basin begins to cascade eastward as a downwelling oceanic equatorial Kelvin wave (EKW). This mechanism often (but not always) plants the seeds for an upcoming El Niño event (Hendon et al. 1999; Kessler and Kleeman 2000; Roundy and Kiladis 2006). In fact, despite what some climate scientists referred to as a ''mega'' downwelling EKW, the much-anticipated 2014 El Niño failed to mature (Menkes et al. 2014; McPhaden 2015). Yet, the 2014 EPac hurricane season was one of the most active on record, with five category-4 and one category-5 TC (according to the Saffir–Simpson hurricane scale; see http://www.aoml.noaa.gov/general/lib/laescae.html for a full description) (Sobel et al. 2016). Two related key questions arise. 1) Is there a link between this abnormally active TC year and the passage of this EKW of substantial amplitude? 2) How much of the EPac warming, favorable for TC intensification, was due to this oceanic wave?

Existing studies addressed the links between atmospheric intraseasonal Kelvin waves, the MJO, and the modulation of TC activity in the EPac and in particular the probability of cyclogenesis (Molinari et al. 1997; Maloney and Hartmann 1998, 2000; Aiyyer and Molinari 2008; Jiang et al. 2012). TC activity at subannual and intraseasonal time scales can be attributed to changes in environmental factors related to MJO events. They generally trigger eastward-propagating atmospheric Kelvin waves that strengthen convection and reinforce MJO zonal westerly wind anomalies over the EPac, which ultimately result in enhanced 850-mb relative vorticity favorable for TC genesis. Overall, convectively active phases of intraseasonal variability can increase the frequency of cyclogenesis by up to fourfold (Barrett and Leslie 2009), mostly through barotropic energy conversion from the mean state to the eddies. The intrinsic predictability of the MJO and atmospheric intraseasonal variability in general is usually around a month (Waliser 2006; Vitart 2009; Kim et al. 2014), which may not be sufficient for forecasting an active TC season well in advance.

In contrast to such atmospheric drivers, oceanic EKWs potentially offer longer prediction lead times as

TABLE 1. Spatial and temporal resolution of the reanalysis products used in this study.

Reanalysis product	Lat resolution	Lon resolution	Time resolution	Period
ORA-S3 (heat content)	1/2°	1°	Monthly outputs	1984–2009
GODAS (heat content)	1/3°	1°	Monthly outputs	1984–2014
ORA-S4 (isotherms 20°C depth)	1/2°	1°	Daily outputs	From 1 Jan 2012 to 13 Oct 2015
ORA-S4 (heat content)	1/2°	1°	Monthly outputs	1984–2014
ERA-Interim (zonal surface wind)	3/4°	3/4°	Monthly average of daily outputs	1984–2014
NOAA–NCEP (OLR)	2 1/2°	2 1/2°	Monthly average of daily outputs	1984–2014

they are continuously generated by subannual and intraseasonal wind forcing in the western Pacific, take about 3–4 months to cross the Pacific basin, and then a couple more months to travel north as coastal trapped waves and reflected westward Rossby waves toward the EPac cyclone-active region. In addition, their nonlinear rectification into the mean state can significantly contribute to the EPac thermocline warming (Wang 2003). In turn, this subsurface warming can potentially modulate TC intensification on subseasonal and annual time scales. The objective of this study is to explore the impact of subsurface ocean warming associated with the passage of these subannual and intraseasonal EKWs on the EPac TC activity and evaluate the potential of such well-monitored oceanic features to improve seasonal and monthly forecasts of hurricane activity with longer lead time.

The rest of this paper is outlined as follows. We first describe the data and our approach in the next section. In section 3, we explore the relationship between seasonal hurricane activity and subsurface temperature variability related to subannual EKWs over the period 1984–2014. In section 4, we focus on the most recent period (2012–15) using daily output from ocean reanalysis to assess the link between EKW intraseasonal variability and the monthly modulation of TC intensity. Conclusions and discussion of our main results are finally presented in section 5.

2. Data and methods

To be consistent with Jin et al. (2014, 2015) and Boucharel et al. (2016), we use oceanic conditions (both at and below the surface) from the European Centre for Medium-Range Weather Forecasts (ECMWF) Ocean Reanalysis System 3 (ORA-S3) that spans the period 1959–2009 (Balmaseda et al. 2008). ORA-S3 has been extensively used and validated (e.g., Zhai and Hu 2013; Jin et al. 2014; Boucharel et al. 2015). One of the motivations of the study is also to understand the particularly active 2014 TC season in the EPac, during which El Niño standard metrics were marginal at best (yet a record TC season emerged), and the even more active 2015 season characterized by the ongoing development of a strong El Niño event. To assess the most recent period, not covered by ORA-S3, we use the National Centers for Environmental Prediction (NCEP) real-time ocean analysis and reanalysis: the new Global Ocean Data Assimilation System (GODAS), over the period 1980–2014 (Behringer and Xue 2004; Saha et al. 2006), as well as the newest version of the ECMWF ocean reanalysis, Ocean Reanalysis System 4 (ORA-S4) (Balmaseda et al. 2013), which is still operational. All ocean products give similar results on their overlapping temporal period, so we present diagnostics performed only over the last 30 years (1984–2014) from an average of these datasets (ensemble average taken over their common period) to smooth out mesoscale features and more clearly identify the EKWs. This reanalysis ensemble mean approach has been used for atmospheric products by Peña-Arancibia et al. (2013) and Boucharel et al. (2016). They point out that the ensemble mean generally outperformed or was nearly as good as any single member. All these products have a monthly temporal resolution (for further details, see Table 1). Second, we use daily output from ORA-S4 over the period from 1 January 2012 to 13 October 2015 to assess the monthly modulation of TC activity by intraseasonal EKW during the particularly active 2014 and 2015 hurricane seasons (section 4).

As an integrated measure of TC activity, we use the accumulated cyclone energy (ACE) index. First, ACE is calculated for individual TC as the sum of the squares of the 1-min maximum sustained surface wind speeds over 35 kt over all 6-h periods during a storm's lifetime (Bell et al. 2000). After obtaining all the individual TC's ACE, the annual ACE (section 3) is integrated over the EPac domain (5°–25°N, 160°–90°W) during the boreal TC season (May–November). In section 4, ACE is calculated monthly, biweekly, and over a 5-day period average over the same domain. We also consider the TC intensity (TCI) since it relates more to oceanic conditions than the ACE, which also encompasses atmospheric effects on storm intensification (Lin and Chan 2015). Similarly, TCI is simply the average of each storm's 1-min maximum sustained surface wind speed during its lifetime. TC data (trajectories and intensity) are obtained from the best-track archives of the National Oceanic and Atmospheric

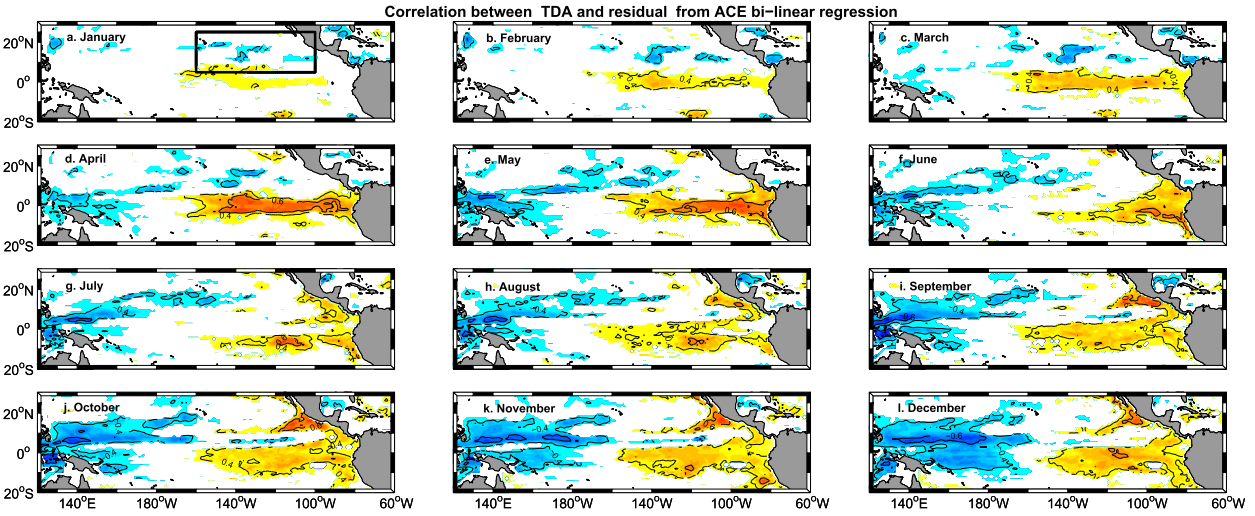

FIG. 1. Significant correlations at the 93% confidence level between annual anomalies of thermocline depth for each calendar month from (a) January to (l) December and the annual residual from the ACE bilinear regression onto Niño-3.4 and T_{sub} [monthly anomalies averaged in the TC region (5°–25°N, 160°–90°W) indicated by the black box in (a), between 5 and 80 m, and during the boreal hurricane season (May–November)]. Contours are 0.2.

Administration's (NOAA's) Tropical Prediction Center (TPC; http://www.nhc.noaa.gov/?epac).

Jin et al. (2014, 2015) use simple bilinear regression statistical models to demonstrate the potential of ENSO subsurface dynamics to be used for interannual predictions of TC activity in the EPac. Jin et al. (2014, 2015) simply express the annual (May–November average) ACE or TCI as a linear combination of the annual Niño-3.4 index [i.e., sea surface temperature (SST) anomalies averaged in the region 5°S–5°N, 170°–120°W] and annual subsurface temperature T_{sub} anomalies averaged in the upper 80 m in the TC region [7°S–17°N, 160°–90°W; cf. Eq. (1)]. Niño-3.4 is assumed to account for the ability of ENSO SST anomalies to alter key atmospheric factors for TC genesis (i.e., TC occurrence frequency) (Dong and Holland 1994; DeMaria 1996; Collins and Mason 2000; Collins 2007; Camargo et al. 2008; Balaguru et al. 2013), while T_{sub} impacts TC intensity and represents the ocean thermal effect of ENSO through meridional redistribution of subsurface heat or, in other words, the RD mechanism (Jin 1997; Jin et al. 2014). Depending on the time period considered (e.g., whether this period is characterized by more frequent EP or CP El Niño types), the fueling effect associated with the ENSO meridional displacement of subsurface heat (i.e., T_{sub}) overall accounts for 30%–50% of the EPac interannual TC activity (Jin et al. 2015):

$$\mathrm{ACE/TCI}_{@\mathrm{May–Nov}} = a\mathrm{Niño3.4}_{@\mathrm{May–Nov}} + bT_{\mathrm{sub}_{@\mathrm{May–Nov}}}, \quad (1)$$

where a and b are the coefficients from the regression on the Niño-3.4 index and T_{sub}, respectively.

In the present study, we focus on the remaining variability of hurricane activity (i.e., the residual unrelated to the interannual ENSO RD mechanism). We simply express the annual residual of TC activity as the difference between either ACE or TCI [left-hand side of Eq. (1)] and the bilinear regressed expression described above [right-hand side of Eq. (1)]; the annual residual time series is shown in Fig. S1 of the supplemental material.

3. Impact of the subannual EKW on the seasonal TC activity

a. Thermocline depth anomalies and TC intensity in the EPac

It has long been recognized that the tropical thermocline provides a waveguide for several types of waves that travel along the equator. The sharp ocean thermal structure in this region (i.e., the shallow thermocline and the strong vertical stratification) facilitates wave propagation with little dissipation (Cane and Sarachik 1977). Thus, we first choose to explore the relationships between the thermocline depth variability in the tropical Pacific, diagnosed as the depth of the 20°C isotherm, and the ACE annual residual in the EPac.

To identify propagations associated with such features and their potential influence on the EPac hurricane activity, we present in Fig. 1 correlation maps (longitude–latitude) between the ACE residual annual time series (cf. Fig. S1 in the supplemental material and section 2) and the annual time series of thermocline depth anomalies (TDAs) from the ocean reanalyzes at each grid point (1° × 1° spatial resolution) and for each

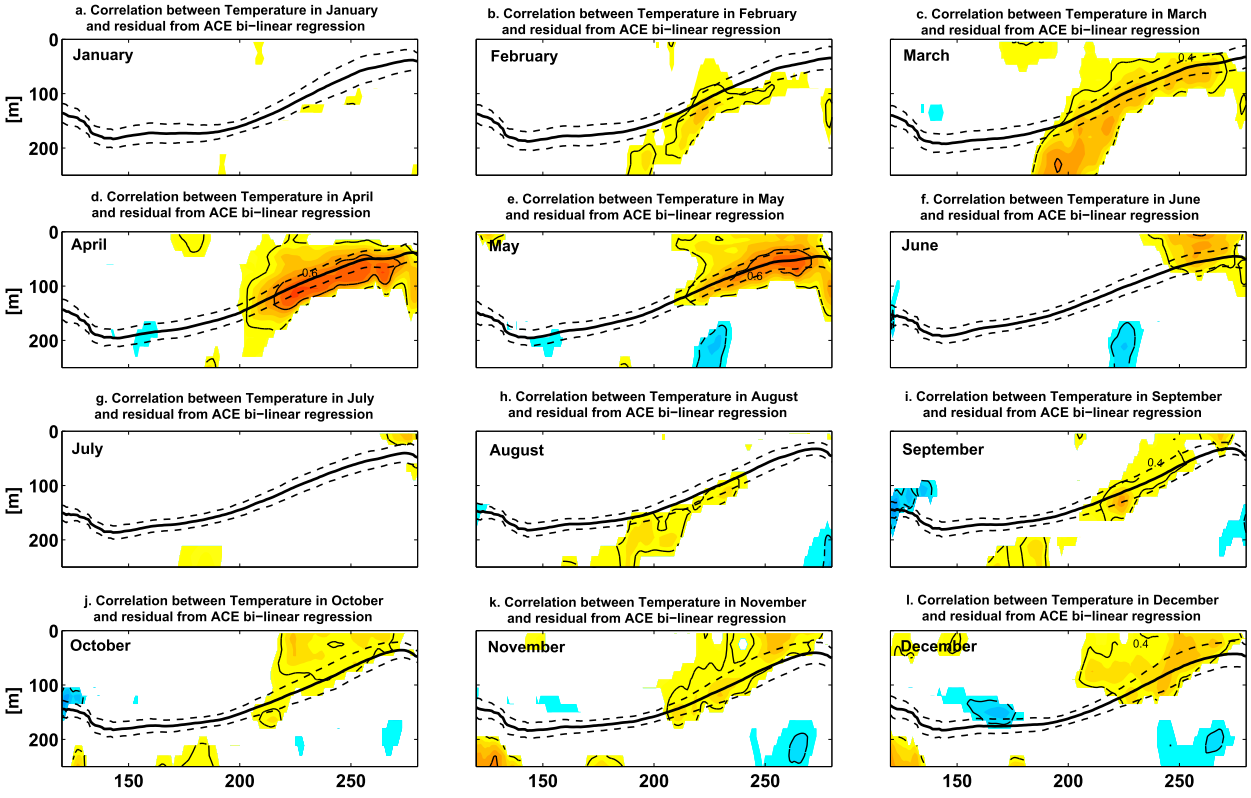

FIG. 2. Equatorial section (averaged between 2.5°S and 2.5°N) of significant correlations at the 93% confidence level between annual anomalies of T_{sub} for each calendar month from (a) January to (l) December and the annual residual from the ACE bilinear regression onto Niño-3.4 and T_{sub} [monthly anomalies averaged in the TC region (5°–25°N, 200°–270°E), between 5 and 80 m, and during the boreal hurricane season (May–November)]. Contours are 0.2. The thicker black line is the corresponding monthly mean thermocline and the dashed black lines represent plus/minus one std dev.

calendar month over the last 30 years (1984–2014). To ensure that TDAs do not include any annual or ENSO variability, we process the anomalies as follows: at each grid point we first remove the monthly mean climatology, and then we remove the regressed Niño-3.4 index.[1] We observe a clear propagation of significant correlations at the 93% confidence level ($r > 0.4$, $p < 0.07$) between TDAs and the ACE annual residual along the equator. This coherent signal originates in the central-western Pacific around January–February (Figs. 1a,b), is fully mature in the central Pacific during March–April (Figs. 1c,d), and then reaches the EPac cold tongue region in May (Fig. 1e), right at the beginning of the boreal hurricane season. Then, this coherent relationship between TDAs and the ACE residual starts spreading poleward along the coast of the Americas (Figs. 1f,g) and reaches the EPac cyclone-active coastal region in July. The signal is subsequently radiated westward from the coast and covers a significant portion of the southeastern EPac TC region between August and December (cf. Figs. 1h,l). This eastward equatorial propagation followed by an off-equatorial westward radiation off the coast of Central America in a specific latitudinal band calls for a careful examination of both the EKW and the reflected Rossby wave signal. Also, the alongshore poleward propagation over a narrow coastal region seems to be a signature of coastal trapped waves (Spillane et al. 1987; Clarke and Shi 1991).

b. *Eastward-propagating EKWs*

We further examine these propagations from the relationship between the ACE residual and the vertical structure of potential temperature anomalies along the equator. Similar to Fig. 1, we present in Fig. 2 vertical

[1] Note that we also tried to remove, with similar outcome, the bilinear regressed Niño-3.4 and Niño-1.2 indices, as well as the bilinear regressed *C* and *E* indices from Takahashi et al. (2011), that is, the first two rotated PCs of SST interannual anomalies representative of the CP and EP El Niño flavor, respectively, so that TDAs do not include any ENSO variability associated with any of these types of events. Results were similar because the oceanic subsurface variability associated with CP events does not have any significant control on the EPac TC activity (Boucharel et al. 2016).

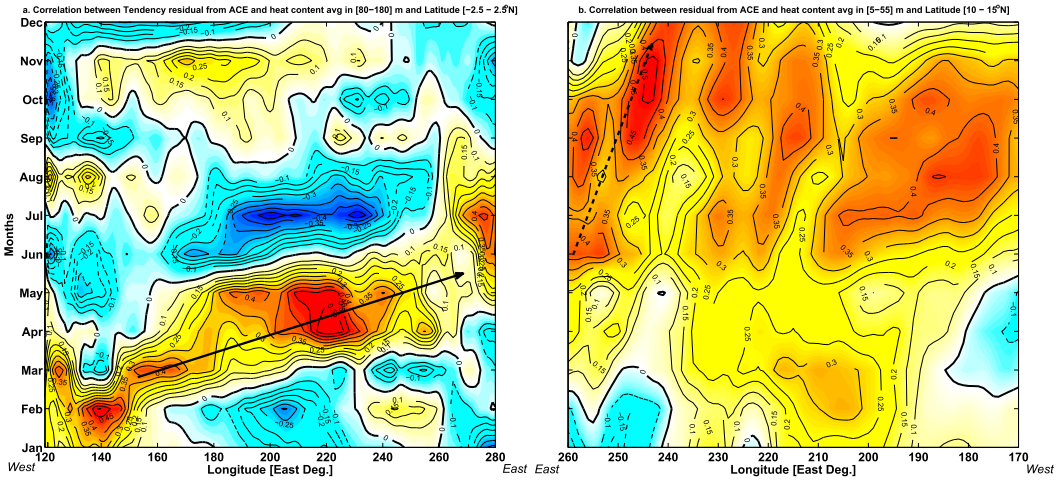

FIG. 3. (a) Time–longitude Hovmöller diagram of correlation between tendency of T_{sub} anomalies (averaged between 2.5°S and 2.5°N and between 80 and 180 m) and the annual residual from the ACE bilinear regression onto Niño-3.4 and T_{sub} [monthly anomalies of temperature averaged in the TC region (10°–15°N, 200°–270°E), between 5 and 80 m, and during the boreal hurricane season]. (b) Time–longitude Hovmöller diagram of correlation between tendency of T_{sub} anomalies in region TC (averaged between 10° and 15°N and between 5 and 55 m) and the annual residual from the similar ACE bilinear regression. Note the reversed sense of the longitude axis to link (a) and (b). Contours are 0.05; the thick black line is the zero contour. Tendency of subsurface temperature anomalies are used to emphasize propagating features and calculated as: $\Delta T_{sub}(\text{month}) = T_{sub}(\text{month}) - T_{sub}(\text{month} - 1)$.

equatorial (2.5°S–2.5°N) sections of correlations between the annual ACE residual and temperature anomalies for each calendar month. Anomalies have been processed similarly to section 3a. Again, there is a clear propagation of significant correlations at the 93% confidence level ($r > 0.4$, $p < 0.07$) along the equatorial thermocline represented by the thick black lines in Fig. 2. The coherent relationship between the subannual variability of subsurface temperature and the ACE annual residual originates around the date line in January–February (Figs. 1a,b) and then propagates along the equatorial thermocline, reaching the EPac cold tongue region in May (Fig. 1e), just in time for the hurricane season, to finally disappear from the equatorial EPac in July (Fig. 1g). At this time, the anomalies of the subsurface temperature (0–50 m) in the equatorial EPac explain almost 40% of the ACE annual residual variability ($r \approx 0.6$) and around 25% of the total variability.

For a more quantitative diagnostic of the propagation, we integrate this coherent signal between 80 and 180 m (to grasp changes happening around the mean thermocline across the entire Pacific basin) and present it in a time–longitude Hovmöller diagram in Fig. 3a. A simple visual inspection shows that the signal takes 3–4 months to cross the basin, indicative of a propagation speed of about 1.9 m s^{-1} (illustrated by the black arrow), consistent with the theoretical phase speed of the first to second baroclinic mode EKW in the eastern equatorial Pacific (Sprintall et al. 2000; Kessler et al. 1995; Picaut and Sombardier 1993). This is further confirmed by a more sophisticated technique that determines probability distributions of zonal phase speeds in a space–time diagram, via the Radon transform (Radon 1917; Challenor et al. 2002; Boucharel et al. 2013). In practice, we project the Hovmöller diagram onto a series of lines at various angles and for different times (Fig. S3a in the supplemental material). This projection in the 2D longitude–time space will reach maximum values when perpendicular to crests (positive correlations) and troughs (negative correlations) in the data. Subsequently, we can identify the angles (i.e., phase speed) for which the maximum projection is attained (Figs. S3b,c in the supplemental material). The ''Radon projection'' pictured in Fig. 3a exhibits a dominant phase speed of 1.55 m s^{-1}. This confirms the strong relationship between the subsurface temperature variability associated with the passage of subannual EKWs and the seasonal TC intensity in the EPac. Note the decrease in positive correlation near 120°W in May–June that can be interpreted in terms of the energy scattering of the EKWs onto the sloping thermocline (Mosquera-Vásquez et al. 2014).

c. *Westward-reflected Rossby wave*

Spillane et al. (1987) used sea level observations to show that poleward-propagating subseasonal variability was detectable along the coast of the Americas from Peru to Central America and California, where the EPac cyclogenesis takes place. Enfield (1987) extended this

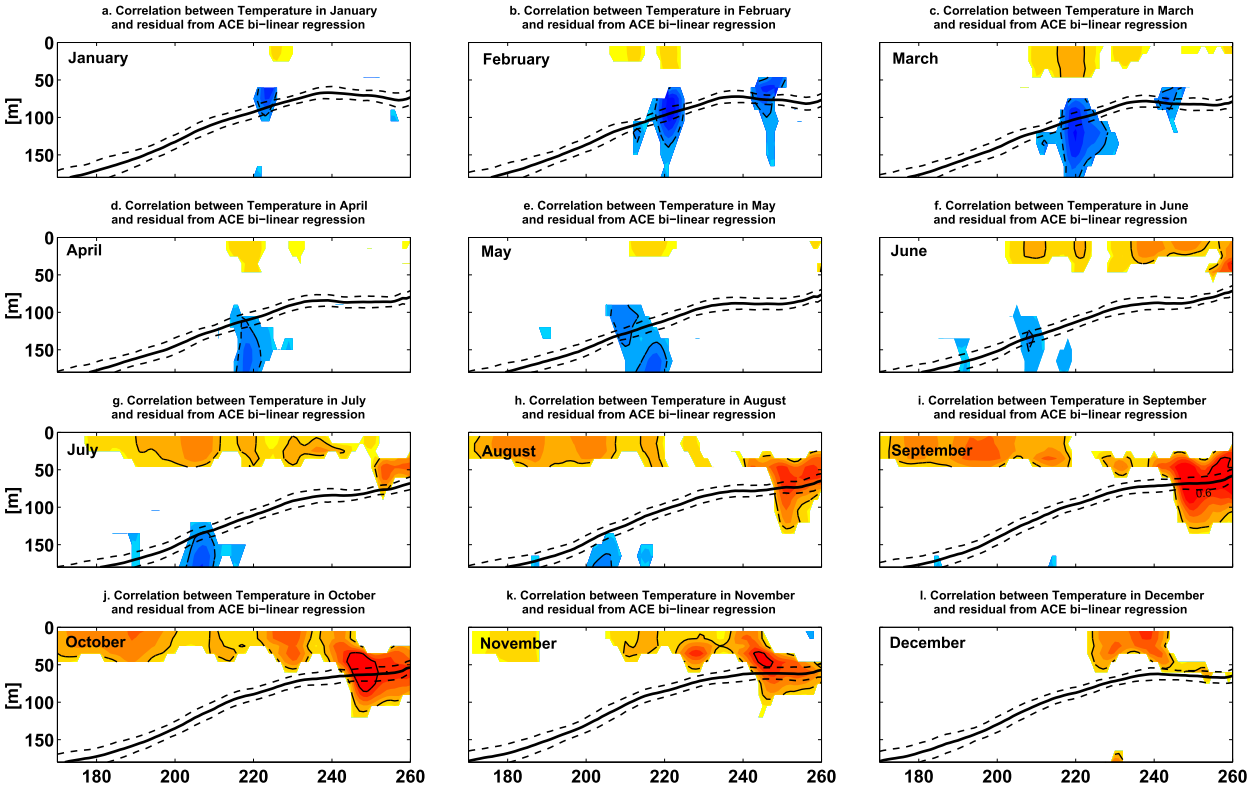

FIG. 4. As in Fig. 2, but for values averaged between 10° and 15°N.

analysis and found that the source of this coastal variability was the first baroclinic mode equatorial Kelvin waves remotely forced by western Pacific winds. When the EKW encounters the eastern boundary, some of its energy is transferred poleward through coastally trapped waves, expanding the equatorial waveguide to higher latitudes in each hemisphere. These coastal Kelvin waves can radiate energy into baroclinic Rossby waves between the equator and 30°S or 30°N, depending on their frequency and the coastline slope (Clarke and Shi 1991). These waves propagate westward along the subtropical thermocline in response to the geostrophic balance (McCreary 1983).

To highlight the propagation of such coherent westward signals between TC intensity and the subsurface heat variability induced by Rossby waves, we present in Fig. 4, similar to Fig. 2 but now averaged between 10° and 15°N, monthly lagged correlations between the ACE annual residual and vertical sections of temperature anomalies. As shown previously (cf. Figs. 2e,f and 3a), the signal between the EKW-induced subsurface anomalies and the hurricane activity in the equatorial EPac reaches the basin's eastern boundary around May–June. The signal starts to appear in the thermocline along the coast of Central America at this time (June–July, cf. Figs. 4f,g) and subsequently spreads westward. The coherency becomes particularly strong ($r > 0.4$, $p < 0.07$) in the EPac cyclone-active and main development region (160°–110°W) between July (Fig. 4g) and October (Fig. 4j) with a well-marked peak in August and September at the heart of the boreal hurricane season.

Again to illustrate the propagation characteristics of this signal, we integrate it between 5 and 55 m (shallow thermocline in the EPac) and present it in a time–longitude Hovmöller diagram in Fig. 3b. Note the reversed sense of the longitude axis in this plot. This analysis shows a clear westward propagation of coherent patterns between the residual hurricane activity and subsurface temperature anomalies associated with the reflected Rossby wave. Visually, we estimate a phase speed around 0.14 m s^{-1} (as shown by the dashed black arrow), with the Radon projection estimation refining this value to 0.26 m s^{-1} (cf. Fig. S4 in the supplemental material). This corresponds roughly to the phase speed predicted by the standard theory for an extratropical freely propagating nondispersive linear first baroclinic Rossby mode around 10°–15°N (i.e., ≈0.20 m s^{-1}; Chelton and Schlax 1996). The variability of subsurface temperature associated with the passage of these waves roughly explains 10%–20% of the yearly variations of TC activity unrelated to ENSO in the EPac ($r \approx 0.40$ in region TC, between 160° and 90°W, and over the TC boreal season, May–November). We also note other westward propagations of positive

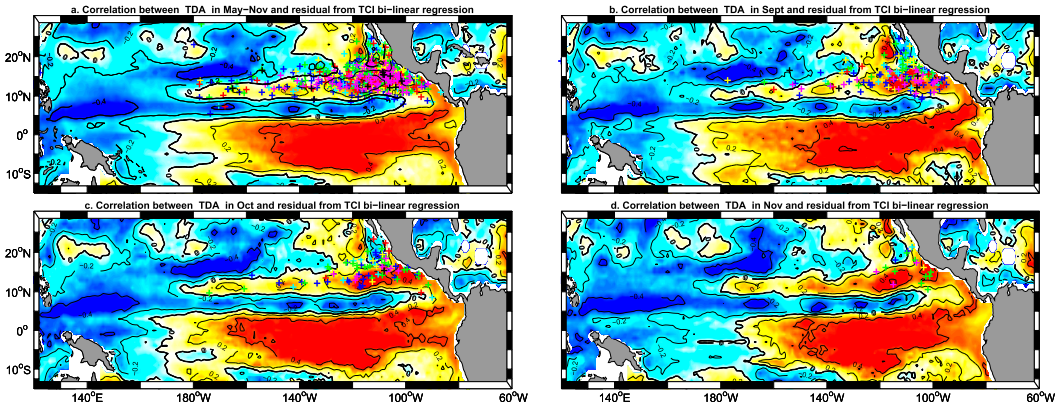

FIG. 5. (a) The max intensification location of all storms that occurred during the Northern Hemisphere hurricane season (May–November) between 1984 and 2014 over the correlations described below averaged over the hurricane season. Tropical depressions are in dark blue, tropical storms are in cyan, category 1 events are in green, category 2 events are in yellow, category 3 events are in red, category 4 events are in magenta, and category 5 events are in black. (b)–(d) Correlations between annual anomalies of thermocline depth for different months—September, October, and November, respectively—and the annual residual from the TCI bilinear regression onto Niño-3.4 and T_{sub}. Contours are 0.2; the thick black line is the zero contour. The colored plus signs represent the location of the strongest intensification (i.e., the location of max increase in wind speed) of every storm that occurred during the corresponding months; for instance, in (b), the plus signs stand for the max intensification location of all TC that occurred in September between 1984 and 2014.

correlation that appear to originate farther away from the coast in the central Pacific (200°–220°E) in June. This can be interpreted as the EKW partial reflection near 120°W onto the zonal density front associated with the shallower thermocline in the east (Mosquera-Vásquez et al. 2014). This might also be the signature of equatorial heat discharge associated with the subannual EKW, that is, a discharge mechanism similar to the one found by Jin et al. (2014), but on subannual time scales. Further analysis based on model experiments would be required to elucidate the mechanisms behind such a westward-propagating variability at 120°W.

The connection between the Rossby wave effect on subsurface variability and the EPac cyclonic intensity is further illustrated in Fig. 5a. It displays the positions of maximum hurricane intensification—defined as the strongest increase in wind speed during the storm lifetime—of all TCs (between 1984 and 2014) over the Rossby wave pattern identified previously. This pattern is defined as the average over the hurricane season (May–November) of the maps corresponding to the monthly lagged correlations between the annual TDA and TCI residual (see Fig. S2 in the supplemental material). Note that we use TCI instead of ACE for this diagnostic because, as mentioned in section 2, TCI is more specifically related to oceanic intensification processes than ACE, which also encompasses atmospheric effects (Lin and Chan 2015). However, similar results are obtained when we use ACE, in particular during the latest part of the TC season, when the Rossby wave signal is fully mature in the EPac (i.e., Fig. S5 in the supplemental material). Most TCs (64% for all categories) and in particular major TCs (74% of category 4 and 5 hurricanes) tend to undergo their maximum intensification over the region of most prominent Rossby wave signature on subsurface temperature. We also repeat the analysis, this time restricting the TC count and the Rossby wave pattern to the individual calendar months of September (Fig. 5b), October (Fig. 5c), and November (Fig. 5d). The westward extent of the Rossby wave pattern along ~10°–12°N fits the hurricanes' location and westward displacement in the EPac. The Rossby wave influence on the subannual subsurface temperature variability can therefore potentially create a warm subsurface water corridor, promoting favorable conditions for TCs to intensify and travel farther west, in particular during the second part of the hurricane season.

4. Modulation of TC intensity by intraseasonal EKWs (2012–15)

a. Propagating mode of oceanic intraseasonal variability

We now explore the effect of intraseasonal subsurface variability due to higher-frequency EKW on the monthly modulation of hurricane intensity during the period 2012–15. The intraseasonal variability associated with atmospheric wave propagation in the tropics is generally assessed through the diagnostics of the 10–90 days

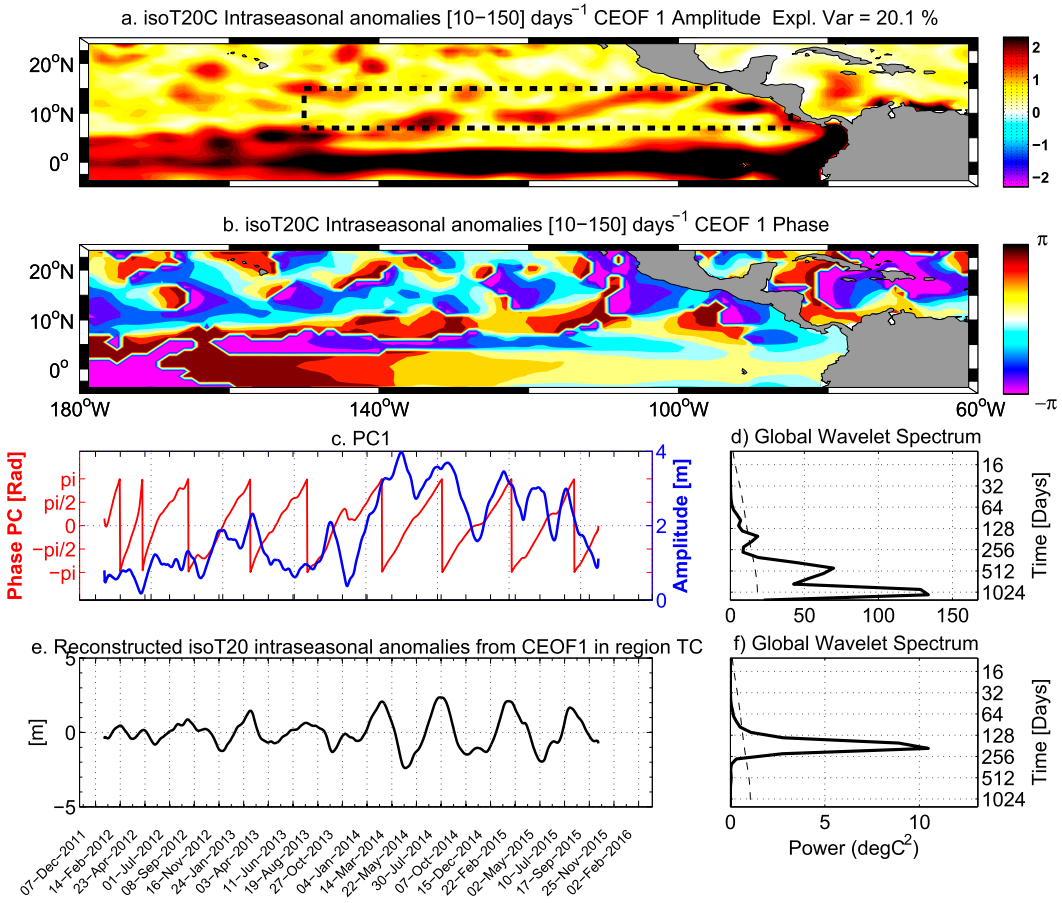

FIG. 6. First mode of the decomposition into CEOFs of intraseasonal (bandpass filtered between 10 and 150 days) anomalies of the 20°C isotherm depth. Shown are the (a) amplitude and (b) phase of the first CEOF spatial pattern. (c) Time series of the corresponding PC, with amplitude in blue and phase in red. (d) Global wavelet spectrum of PC1 amplitude. (e) Time series of the intraseasonal anomalies of the 20°C isotherm averaged in the region delineated by the thick dashed line in (a) and reconstructed from the first CEOF mode only. The results are presented for the central to eastern North Pacific but the CEOF decomposition is performed over the entire tropical Pacific (25°N–25°S, 120°E–60°W).

bandpass-filtered anomalies (Jiang et al. 2012). However, in the Pacific, Kessler et al. (1995) and Cravatte et al. (2003) have shown the presence of an energetic peak of oceanic variability at 120 days in sea level. Therefore, in this context, we choose to define the intraseasonal TDA as the 10–150 days bandpass-filtered (first-order Butterworth filter) anomalies of isotherm 20°C daily output from ORA-S4 (see section 2).

Complex empirical orthogonal functions (CEOFs) provide an efficient tool to disentangle the spatiotemporal characteristics of the intraseasonal TDA. In particular, by providing both amplitude and phase information, CEOFs are well suited to capturing propagating features (Barnett 1983; Stein et al. 2011; Boucharel et al. 2013). Here we conduct a CEOF analysis of the intraseasonal TDA over the period from 1 January 2012 to 13 October 2015 and over the whole tropical Pacific. The resulting first CEOF mode (CEOF1) is shown in Fig. 6. CEOF1 explains 20% of the thermocline depth intraseasonal variability and is characterized by strong amplitude along the equator (Fig. 6a) associated with an eastward propagation (see the decrease in phase along the equator from west to east in Fig. 6b). There is also a pattern of significant amplitude along the coast of Central America propagating poleward, as well as in the EPac cyclone-active region (delineated by the dashed black box in Fig. 6a) that propagates westward. This is the exact same signature as the subannual equatorial Kelvin, coastal trapped, and Rossby waves triplet identified in the previous section, but evidenced here on intraseasonal time scales. The principal component (PC) of CEOF1 is

split into an amplitude and phase time series, shown in blue and red in Fig. 6c, respectively. The phase exhibits a constant decrease, indicative of a dominant eastward propagation over the period 2012–15, as the wave signature is stronger along the equator (EKW). The spectral properties of the first principal component (PC1) are diagnosed by performing a wavelet decomposition in Fig. 6d (Torrence and Compo 1998). The more prominent peak, around 2.5 years, is most likely due to the amplitude modulation of intraseasonal EKW activity in the EPac, as part of the low-frequency evolution of the tropical Pacific mean state (Dewitte et al. 2008), with little (enhanced) activity in 2012–13 (2014–15). The second significant peak is found in the 120–130 days period, and is the clearly dominant time scale in the TDA signal reconstructed in the EPac (dashed black box in Fig. 6a) from CEOF1 only (Figs. 6d,f). We consider, for more completeness, the second and third CEOF modes, and present similar diagnostics for CEOF1, CEOF2, and CEOF3, which altogether explain 30% of the intraseasonal variability (Fig. S6 in the supplemental material). The amplitude and phase patterns are essentially the same, but the peak of variability tends to broaden toward higher frequency and become significant in the 90–130 days band. In addition, the frequency range of TDA variability found in the EPac is coherent with the latitudinal dependency of the dominant frequency radiated westward (i.e., not coastally trapped), around 90–180 days between 9° and 15°N (Clarke and Shi 1991). The first three modes of intraseasonal TDA variability in the EPac, and CEOF1 to a great extent capture the propagative signal of the eastward EKW and reflected off-equatorial Rossby wave. At this stage, one can wonder if such small deviations in thermocline depth variability (~2–6 m depending on the number of CEOF modes considered) can significantly contribute to subsurface temperature anomalies and ultimately promote substantial variations in hurricane intensity. This is actually the case due to the sharp thermocline in the EPac, which can produce a large rate of temperature changes within the upper layer through anomalous vertical advection of mean temperature. For instance, Jin et al. (2014) showed that between periods of recharged and discharged subsurface temperature in this region, characterized by subsurface temperature changes around 5°C, the variation in thermocline depth is less than 15 m (see Fig. 23 of their supplemental material). Yet the total (major; i.e., category 3 and above) hurricanes count between these periods was increased up to 74% (350%). This suggests a high sensitivity of TC activity to changes in vertical oceanic structure in this region.

b. *Relationships between oceanic intraseasonal variability and monthly TC activity*

We compare the amplitude of TDA PC1 to 5-day mean, biweekly, and monthly values of ACE and TCI averaged over the region delineated in Fig. 6a. The time series are presented in Fig. 7 and restricted only to the boreal hurricane season (May–November) for clarity. Not unexpectedly, there is no evident link between the 5-day mean hurricane intensity and the intraseasonal wave activity, with low correlations of 0.26 (0.23) between TCI (ACE) and the amplitude of PC1, as our bandpass filtering has smoothed the high-frequency variability out. Yet, PC1 amplitude is clearly in phase with the monthly time series of ACE and TCI and more surprisingly to some extent with the biweekly time series as well, with correlations of 0.56 and 0.45 for TCI, and 0.54 and 0.43 for ACE, respectively, all significant at the 95% level. This connection becomes even clearer when we consider the PC associated with the first three CEOF modes (Fig. S6 in the supplemental material). The consideration of three modes allows grasping more of the westward propagation variance through the inclusion of a wider range of periods at which the Rossby wave can radiate at such latitudes (cf. Figs. S6d,f in the supplemental material and Figs. 6d,f). The relationship between the oceanic intraseasonal variability and TC activity seems even stronger during the 2014 and 2015 hurricane season as the intraseasonal EKW activity is significantly increased (cf. blue line in Fig. 6c).

To understand this connection between hurricane intensity and wave activity in a dynamical framework, we collocate, in a similar fashion to Fig. 5, TC trajectories with composites of reconstructed TDA for CEOF1–CEOF3. In Fig. 8a, the shading represents the reconstructed intraseasonal TDA signal averaged between May and August (i.e., the downwelling phase of the intraseasonal Rossby wave) and the spaghetti lines denote the TC tracks restricted to their maximum intensification part, that is, between the moment of strongest increase in wind speed until the maximum wind speed is attained, for all storms that occurred between May and August (for 2012–15). Red shading indicates a deeper thermocline, and thus higher heat content. There is a good match between the location where positive subsurface ocean anomalies are found and the location of TC strengthening. Most tropical storms tend to build up and reach their maximum intensity over patches of anomalously deep intraseasonal thermocline (i.e., higher heat content). In particular, the downwelling Rossby wave passage and its imprint on subsurface characteristics along ~10°–12°N seems to provide a warm water pathway that significantly contributes to the westward hurricanes translation. Likewise, Fig. 8b represents

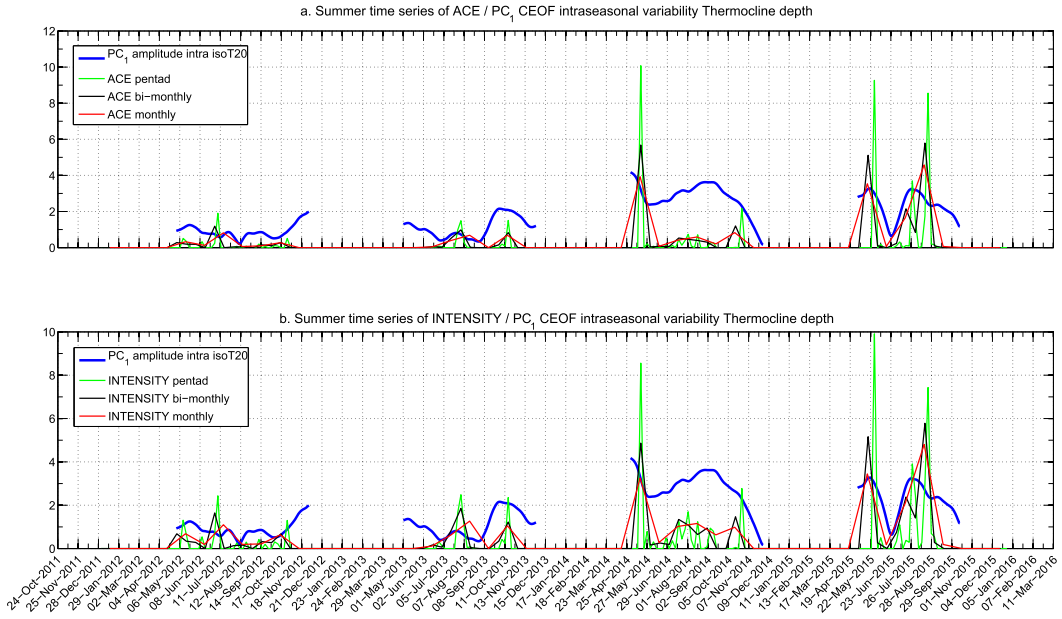

FIG. 7. Hurricane season (May–November) time series of the standardized (a) ACE and (b) TCI averaged in the region shown in Fig. 6a (dashed box) at different temporal resolution (5-day average in green, 2-week average in black, and monthly average in red) and hurricane season time series of the PC amplitude from the first CEOF mode of intraseasonal TDA (thick blue) from 1 Jan 2012 to 13 Oct 2015.

the reconstructed intraseasonal TDA signal averaged between September and November (i.e., the upwelling phase of the intraseasonal Rossby wave) and the lines are TCs trajectory that occurred between September and November. In contrast, when the wave passage promotes a shoaling of the intraseasonal TDA (upwelling phase; Fig. 8b), the upper-ocean properties are detrimental to hurricane intensification and limit their westward extent. Instead, TCs tend to be more confined along the coast of Central America.

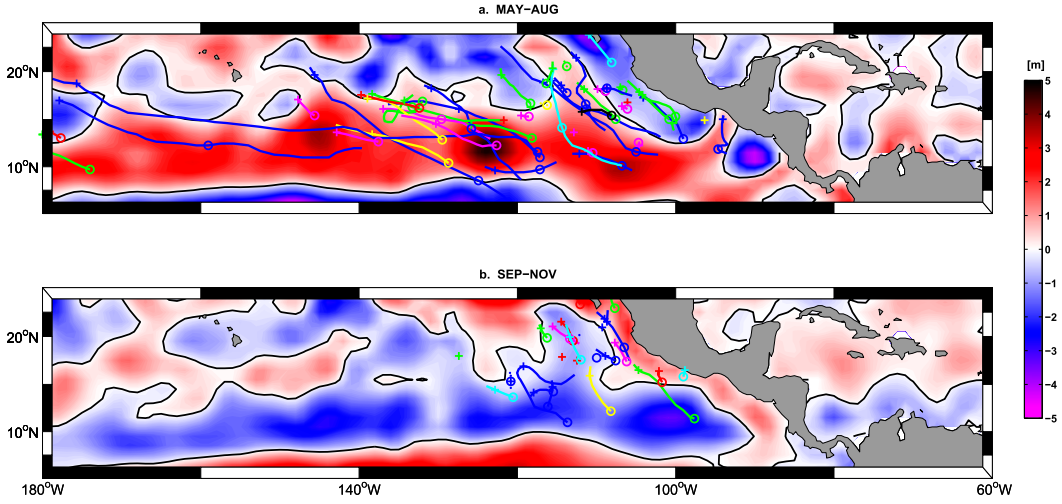

FIG. 8. Composites of reconstructed intraseasonal anomalies of thermocline depth (m) from the first three CEOF modes. (a) Average over the Rossby wave downwelling phase (May–August) and (b) average over the upwelling phase (September–November). Red (positive) patches represent deeper than usual thermocline (i.e., higher heat content). The colored lines represent the TCs trajectories that occurred during the corresponding month between the time of their max intensification (i.e., max wind speed increase) represented by the colored circles until their max wind speed is attained, represented by the plus signs. Tropical depressions are in dark blue, tropical storms are in cyan, category 1 events are in green, category 2 events are in yellow, category 3 events are in red, category 4 events are in magenta, and category 5 events are in black.

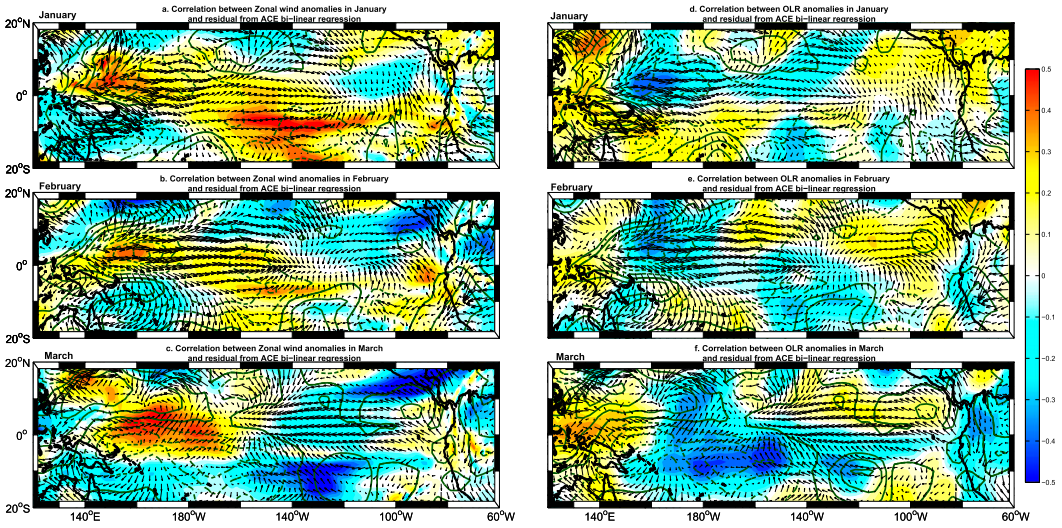

FIG. 9. Correlations between annual high-pass-filtered (with cutoff frequency of 6 months^{-1}) anomalies of surface zonal wind (at the 850-mb atmospheric level) for different calendar months—(a) January, (b) February, and (c) March—and the annual residual from the ACE bilinear regression onto Niño-3.4 and T_{sub} [monthly anomalies of temperature averaged in the TC region (5°–25°N, 160°–90°W), between 5 and 80 m, and during the hurricane season (May–November)]. Arrows represent vectors of high-pass-filtered surface wind anomalies averaged over the corresponding month. Green plain (dashed) lines are positive (negative) high-pass-filtered anomalies of OLR averaged over the corresponding month. Contours are 0.2 W m^{-2}. (d)–(f) As in (a)–(c), but for the correlations between annual high-pass-filtered anomalies of OLR for different calendar months and the annual residual from the ACE bilinear regression.

Our results indicate that the high intraseasonal wave activity in 2014 and 2015 seems to have played a major role in both the overall high seasonal hurricane activity and its monthly modulation.

5. Summary and conclusions

The impact of subseasonal oceanic variability on the EPac hurricane activity is studied here using oceanic reanalysis and the TPC best-track archive. We take advantage of the inclusion of Argo float data into reanalysis products to ensure a more realistic simulation of the oceanic vertical structure (Gould et al. 2004) and the recent body of studies highlighting a tight connection between upper-ocean properties and TC intensity (e.g., Jin et al. 2014, 2015; Boucharel et al. 2016; Vincent et al. 2014; Balaguru et al. 2013; Lin et al. 2013; Price 2009) to focus on the effect of subsurface equatorial dynamics on the EPac hurricane activity. In particular, we determine how much the thermocline warming associated with the passage of subannual and intraseasonal EKW can participate in the seasonal and monthly modulation of TC activity in this basin.

By performing monthly lag correlations between the annual oceanic properties and residual of hurricane activity unrelated to ENSO air–sea coupled dynamics, we were able to identify subannual basin-scale propagations that are significantly linked to TC intensity in the EPac. These oceanic waves have a marked signature on the upper-ocean vertical structure (TDA and heat content), in particular in the EPac cyclone-active region during the boreal hurricane season. Similar to the remote and delayed influence of ENSO equatorial heat discharge on TC interannual activity (Jin et al. 2014, 2015; Boucharel et al. 2016), the oceanic equatorial subannual variability that originates in the western Pacific in boreal winter seems to exert a strong control on the annual variation of hurricane intensity, explaining up to 30% of the ACE residual, which represents around 15%–20% of the total TC activity. The time scales involved in the EKW propagation allow anticipating their influence on subsurface temperature variability and the subsequent ''storm fueling'' effect at least a few months in advance, thereby offering a potential considerable lead time to predict the seasonal TC intensity in the EPac. As a consistency check, we have also assessed to what extent the subannual atmospheric variability in the western Pacific in boreal winter, assumed to trigger such EKWs, is related to the EPac TC intensity. Similarly to Figs. 1, 2, and 4, Fig. 9 shows monthly-lagged correlation maps between the ACE annual residual and the annual high-pass-filtered anomalies (using a first-order Butterworth filter with a 6 months^{-1} cutoff frequency) of surface zonal wind (at the 850-mb atmospheric level) from ERA-Interim (Dee et al. 2011) for the boreal winter calendar months (period 1984–2014). There is a high

correlation between the annual modulation of intraseasonal surface wind anomalies and the ACE residual initiating to the west of the Maritime Continent in January and further propagating eastward toward the central western Pacific (around the international date line) in March. This signal is accompanied by the eastward propagation of negative intraseasonal anomalies of outgoing longwave radiation (OLR) (dashed green lines in Figs. 9d–f). OLR data come from NOAA–NCEP (Liebmann and Smith 1996) and negative OLR anomalies are a good indicator of enhanced deep convective activity. Regardless of the complex intricacy of mechanisms that trigger EKWs (Puy et al. 2015), this confirms the considerable lead time to anticipate the intensity of the boreal TC season: up to 3–6 months in advance, when EKW are generated in boreal winter in the western Pacific.

The use of daily output of thermocline depth enabled us to investigate the impact of higher-frequency oceanic variability on EPac hurricane activity. Although restricted to a short time period, the analysis highlights the monthly modulation of TC intensity by the intraseasonal EKW activity, and emphasizes the strong forecasting potential of such oceanic variability. Interestingly, this effect is mostly captured by the first propagative mode of the CEOF decomposition. This offers a robust framework to embed the hurricane ''fueling effect'' by intraseasonal subsurface anomalies within the more general basin-scale equatorial dynamics. The spatial distribution of hurricane maximum intensification tends to follow the intraseasonal TDA field projected onto the EKW/Rossby wave amplitude pattern. Indeed, the patches of positive TDA (i.e., deeper thermocline, decreased mixed layer stratification, and increased upper-layer temperature) seem to provide an oceanic pathway by offering warm subsurface water crucial for hurricane strengthening. This also suggests that this oceanic mechanism of intraseasonal variability can potentially contribute to the operational tracking of individual TC. Overall, this study draws attention to the relationship between the EPac TC activity and the equatorial subsurface ocean dynamics at intraseasonal time scales, extending the study by Jin et al. (2014, 2015) and Boucharel et al. (2016). It also emphasizes the potential of such deterministic oceanic mechanisms for hurricane predictions. In this regard, it would be interesting to evaluate if statistical forecasts of subseasonal TC activity based on these processes of intraseasonal variability can exceed the skill and lead time (around 20 days) of dynamical forecasts of atmospheric model, such as those of Vitart (2009). This would require further investigation on the triggering of the intraseasonal extratropical Rossby wave around 10°–15°N in the EPac, such as the respective role of remote (EKW) versus local (wind) forcing. Also, the TC region is characterized by high values of eddy kinetic energy, which implies a likely interaction between the linear Rossby wave and mesoscale activity. In addition, due to the relatively limited time period considered to emphasize the potential predictive value of our results, it calls for investigating similar mechanisms in a long-term coupled simulation in a TC-permitting model (e.g., HiRAM; Camargo et al. 2014).

Acknowledgments. This project was supported by the Australian Research Council (FL100100214); U.S. National Science Foundation Grants ATM1034798, ATM1049219, and ATM1406601; U.S. Department of Energy Grant DESC005110; U.S. NOAA Grant NA10OAR4310200; the China Meteorological Special Project (GYHY201206033); and the 973 Program of China (2010CB950404 and 2013CB430203). I.I.L.'s work is supported by Taiwan's Ministry of Science and Technology under Grants NSC 101-2111-M-002-002-MY2, NSC 101-2628-M-002-001-MY4, and 102R7803. Three anonymous reviewers are thanked for their constructive comments.

REFERENCES

Aiyyer, A., and J. Molinari, 2008: MJO and tropical cyclogenesis in the Gulf of Mexico and eastern Pacific: Case study and idealized numerical modeling. *J. Atmos. Sci.*, **65**, 2691–2704, doi:10.1175/2007JAS2348.1.

Ashok, K., S. K. Behera, S. A. Rao, H. Weng, and T. Yamagata, 2007: El Niño Modoki and its possible teleconnection. *J. Geophys. Res.*, **112**, C11007, doi:10.1029/2006JC003798.

Balaguru, K., R. L. Leung, and J.-H. Yoon, 2013: Oceanic control of northeast Pacific hurricane activity at interannual timescales. *Environ. Res. Lett.*, **8**, 044009, doi:10.1088/1748-9326/8/4/044009.

Balmaseda, M. A., A. Vidard, and D. L. T. Anderson, 2008: The ECMWF Ocean Analysis System: ORA-S3. *Mon. Wea. Rev.*, **136**, 3018–3034, doi:10.1175/2008MWR2433.1.

——, K. Mogensen, and A. Weaver, 2013: Evaluation of the ECMWF Ocean Reanalysis System ORAS4. *Quart. J. Roy. Meteor. Soc.*, **139**, 1132–1161, doi:10.1002/qj.2063.

Barnett, T. P., 1983: Interaction of the monsoon and Pacific trade wind system at interannual timescales. Part I: The equatorial zone. *Mon. Wea. Rev.*, **111**, 756–773, doi:10.1175/1520-0493(1983)111<0756:IOTMAP>2.0.CO;2.

Barrett, B. S., and L. M. Leslie, 2009: Links between tropical cyclone activity and Madden–Julian oscillation phase in the North Atlantic and northeast Pacific basins. *Mon. Wea. Rev.*, **137**, 727–744, doi:10.1175/2008MWR2602.1.

Battisti, D. S., and A. C. Hirst, 1989: Interannual variability in a tropical atmosphere–ocean model: Influence of the basic state, ocean geometry and nonlinearity. *J. Atmos. Sci.*, **46**, 1687–1712, doi:10.1175/1520-0469(1989)046<1687:IVIATA>2.0.CO;2.

Behringer, D. W., and Y. Xue, 2004: Evaluation of the Global Ocean Data Assimilation System at NCEP: The Pacific Ocean. *Eighth Symp. on Integrated Observing and Assimilation Systems for Atmosphere, Oceans, and Land Surface*,

Seattle, WA, Amer. Meteor. Soc., 11–15. [Available online at https://ams.confex.com/ams/pdfpapers/70720.pdf.]

Bell, G. D., and Coauthors, 2000: Climate assessment for 1999. *Bull. Amer. Meteor. Soc.*, **81**, S1–S50, doi:10.1175/1520-0477(2000)81[s1:CAF]2.0.CO;2.

Boucharel, J., A. Timmermann, and F.-F. Jin, 2013: Zonal phase propagation of ENSO sea surface temperature anomalies: Revisited. *Geophys. Res. Lett.*, **40**, 4048–4053, doi:10.1002/grl.50685.

——, ——, A. Santoso, M. H. England, F.-F. Jin, and M. A. Balmaseda, 2015: A surface layer variance heat budget for ENSO. *Geophys. Res. Lett.*, **42**, 3529–3537, doi:10.1002/2015GL063843.

——, F.-F. Jin, I. I. Lin, S.-C. Huang, and M. H. England, 2016: Different control of tropical cyclone activity in the eastern Pacific for two types of El Niño. *Geophys. Res. Lett.*, **43**, 1679–1686, doi:10.1002/2016GL067728.

Busalacchi, A. J., and J. J. O'Brien, 1980: The seasonal variability in a model of the tropical Pacific. *J. Phys. Oceanogr.*, **10**, 1929–1951, doi:10.1175/1520-0485(1980)010<1929:TSVIAM>2.0.CO;2.

Camargo, S. J., A. W. Robertson, A. G. Barnston, and M. Ghil, 2008: Clustering of eastern North Pacific tropical cyclone tracks: ENSO and MJO effects. *Geochem. Geophys. Geosyst.*, **9**, Q06V05, doi:10.1029/2007GC001861.

——, M. K. Tippett, A. H. Sobel, G. A. Vecchi, and M. Zhao, 2014: Testing the performance of tropical cyclone genesis indices in future climates using the HiRAM model. *J. Climate*, **27**, 9171–9196, doi:10.1175/JCLI-D-13-00505.1.

Cane, M. A., and E. S. Sarachik, 1977: Forced baroclinic ocean motions: III. The linear equatorial basin case. *J. Mar. Res.*, **37**, 355–398.

——, M. Münnich, and S. E. Zebiak, 1990: A study of self-excited oscillations of the tropical ocean–atmosphere system. Part I: Linear analysis. *J. Atmos. Sci.*, **47**, 1562–1577, doi:10.1175/1520-0469(1990)047<1562:ASOSEO>2.0.CO;2.

Challenor, P. G., P. Cipollini, and D. Cromwell, 2002: Use of the 3D Radon transform to examine the properties of oceanic Rossby waves. *J. Atmos. Oceanic Technol.*, **18**, 1558–1566, doi:10.1175/1520-0426(2001)018<1558:UOTRTT>2.0.CO;2.

Chelton, D. B., and M. G. Schlax, 1996: Global observations of oceanic Rossby waves. *Science*, **272**, 234–238, doi:10.1126/science.272.5259.234.

Clarke, A. J., and C. Shi, 1991: Critical frequencies at ocean boundaries. *J. Geophys. Res.*, **96**, 10 731–10 738, doi:10.1029/91JC00933.

Collins, J. M., 2007: The relationship of ENSO and relative humidity to interannual variations of hurricane frequency in the northeast Pacific Ocean. *Pap. Appl. Geogr. Conf.*, **30**, 324–333.

——, and I. M. Mason, 2000: Local environmental conditions related to seasonal tropical cyclone activity in the northeast Pacific basin. *Geophys. Res. Lett.*, **27**, 3881–3884, doi:10.1029/2000GL011614.

Cravatte, S., J. Picaut, and G. Eldin, 2003: Second and first baroclinic Kelvin modes in the equatorial Pacific at intraseasonal timescales. *J. Geophys. Res.*, **108**, 3266, doi:10.1029/2002JC001511.

Dee, D. P., and Coauthors, 2011: The ERA-Interim reanalysis: Configuration and performance of the data assimilation system. *Quart. J. Roy. Meteor. Soc.*, **137**, 553–597, doi:10.1002/qj.828.

DeMaria, M., 1996: The effect of vertical shear on tropical cyclone intensity change. *J. Atmos. Sci.*, **53**, 2076–2087, doi:10.1175/1520-0469(1996)053<2076:TEOVSO>2.0.CO;2.

Dewitte, B., S. Purca, S. Illig, L. Renault, and B. S. Giese, 2008: Low-frequency modulation of intraseasonal equatorial Kelvin wave activity in the Pacific from SODA: 1958–2001. *J. Climate*, **21**, 6060–6069, doi:10.1175/2008JCLI2277.1.

Dong, K., and G. J. Holland, 1994: A global view of the relationships between ENSO and tropical cyclone frequencies. *J. Meteor. Res.*, **8**, 19–29.

Enfield, D. B., 1987: The intraseasonal oscillation in eastern Pacific sea levels: How is it forced? *J. Phys. Oceanogr.*, **17**, 1860–1876, doi:10.1175/1520-0485(1987)017<1860:TIOIEP>2.0.CO;2.

Gould, J., and Coauthors, 2004: Argo profiling floats bring new era of in situ ocean observations. *Eos, Trans. Amer. Geophys. Union*, **85**, 185–191, doi:10.1029/2004EO190002.

Gushchina, D., and B. Dewitte, 2012: Intraseasonal tropical atmospheric variability associated with the two flavors of El Niño. *Mon. Wea. Rev.*, **140**, 3669–3681, doi:10.1175/MWR-D-11-00267.1.

Harrison, D. E., and N. K. Larkin, 1998: El Niño–Southern Oscillation sea surface temperature and wind anomalies, 1946–1993. *Rev. Geophys.*, **36**, 353–399, doi:10.1029/98RG00715.

Hendon, H. H., B. Liebmann, and J. D. Glick, 1999: Interannual variability of the Madden–Julian oscillation during austral summer. *J. Climate*, **12**, 2538–2550, doi:10.1175/1520-0442(1999)012<2538:IVOTMJ>2.0.CO;2.

Jauregui, E., 2003: Climatology of landfalling hurricanes and tropical storms in Mexico. *Atmósfera*, **16** (4), 193–204.

Jiang, X., M. Zhao, and D. E. Waliser, 2012: Modulation of tropical cyclones over the eastern Pacific by intraseasonal variability simulated in an AGCM. *J. Climate*, **25**, 6524–6538, doi:10.1175/JCLI-D-11-00531.1.

Jin, F.-F., 1997: An equatorial ocean recharge paradigm for ENSO. Part I: Conceptual model. *J. Atmos. Sci.*, **54**, 811–829, doi:10.1175/1520-0469(1997)054<0811:AEORPF>2.0.CO;2.

——, J. Boucharel, and I.-I. Lin, 2014: Eastern Pacific tropical cyclones intensified by El Niño delivery of subsurface ocean heat. *Nature*, **516**, 82–85, doi:10.1038/nature13958.

——, ——, and ——, 2015: Jin et al. reply. *Nature*, **526**, doi:10.1038/nature15547.

Johnson, N. C., 2013: How many ENSO flavors can we distinguish? *J. Climate*, **26**, 4816–4827, doi:10.1175/JCLI-D-12-00649.1.

Kessler, W. S., and R. Kleeman, 2000: Rectification of the Madden–Julian oscillation into the ENSO cycle. *J. Climate*, **13**, 3560–3575, doi:10.1175/1520-0442(2000)013<3560:ROTMJO>2.0.CO;2.

——, M. J. McPhaden, and K. M. Weickmann, 1995: Forcing of intraseasonal Kelvin waves in the equatorial Pacific Ocean. *J. Geophys. Res.*, **100**, 10 613–10 631, doi:10.1029/95JC00382.

Kim, H. M., P. J. Webster, V. E. Toma, and D. Kim, 2014: Predictability and prediction skill of the MJO in two operational forecasting systems. *J. Climate*, **27**, 5364–5378, doi:10.1175/JCLI-D-13-00480.1.

Liebmann, B., and C. A. Smith, 1996: Description of a complete (interpolated) outgoing longwave radiation dataset. *Bull. Amer. Meteor. Soc.*, **77**, 1275–1277.

Lin, I.-I., and J. C. L. Chan, 2015: Recent decrease in typhoon destructive potential and global warming implications. *Nat. Commun.*, **6**, 7182, doi:10.1038/ncomms8182.

——, and Coauthors, 2013: An ocean coupling potential intensity index for tropical cyclones. *Geophys. Res. Lett.*, **40**, 1878–1882, doi:10.1002/grl.50091.

Madden, R. A., and P. R. Julian, 1994: Observations of the 40–50-day tropical oscillation—A review. *Mon. Wea. Rev.*, **122**, 814–837, doi:10.1175/1520-0493(1994)122<0814:OOTDTO>2.0.CO;2.

Maloney, E. D., and D. L. Hartmann, 1998: Frictional moisture convergence in a composite life cycle of the Madden–Julian oscillation. *J. Climate*, **11**, 2387–2403, doi:10.1175/1520-0442(1998)011<2387:FMCIAC>2.0.CO;2.

——, and ——, 2000: Modulation of eastern North Pacific hurricanes by the Madden–Julian oscillation. *J. Climate*, **13**, 1451–1460, doi:10.1175/1520-0442(2000)013<1451:MOENPH>2.0.CO;2.

McCreary, J. P., 1983: A model for tropical ocean–atmosphere interaction. *Mon. Wea. Rev.*, **111**, 370–387, doi:10.1175/1520-0493(1983)111<0370:AMOTOA>2.0.CO;2.

McPhaden, M. J., 2015: Playing hide and seek with El Niño. *Nat. Climate Change*, **5**, 791–795, doi:10.1038/nclimate2775.

Menkes, C. E., M. Lengaigne, J. Vialard, M. Puy, P. Marchesiello, S. Cravatte, and G. Cambon, 2014: About the role of westerly wind events in the possible development of an El Niño in 2014. *Geophys. Res. Lett.*, **41**, 6476–6483, doi:10.1002/2014GL061186.

Molinari, J., D. Knight, M. Dickinson, D. Vollaro, and S. Skubis, 1997: Potential vorticity, easterly waves, and eastern Pacific tropical cyclogenesis. *Mon. Wea. Rev.*, **125**, 2699–2708, doi:10.1175/1520-0493(1997)125<2699:PVEWAE>2.0.CO;2.

Mosquera-Vásquez, K., B. Dewitte, and S. Illig, 2014: The central Pacific El Niño intraseasonal Kelvin wave. *J. Geophys. Res.*, **119**, 6605–6621, doi:10.1002/2014JC010044.

Murakami, H., B. Wang, T. Li, and A. Kitoh, 2013: Projected increase in tropical cyclones near Hawaii. *Nat. Climate Change*, **3**, 749–754, doi:10.1038/nclimate1890.

Neelin, J. D., D. S. Battisti, A. C. Hirst, F.-F. Jin, Y. Wakata, T. Yamagata, and S. E. Zebiak, 1998: ENSO theory. *J. Geophys. Res.*, **103**, 14 261–14 290, doi:10.1029/97JC03424.

Peduzzi, P. B., and Coauthors, 2012: Global trends in tropical cyclone risk. *Nat. Climate Change*, **2**, 289–294, doi:10.1038/nclimate1410.

Peña-Arancibia, J. L., A. I. J. M. Van Dijk, L. J. Renzullo, and M. Mulligan, 2013: Evaluation of precipitation estimation accuracy in reanalyses, satellite products and an ensemble method for regions in Australia and South and East Asia. *J. Hydrometeor.*, **14**, 1323–1333, doi:10.1175/JHM-D-12-0132.1.

Picaut, J., and L. Sombardier, 1993: Influence of density stratification and bottom depth on vertical mode structure functions in the tropical Pacific. *J. Geophys. Res.*, **98**, 14 727–14 737, doi:10.1029/93JC00885.

Price, J. F., 2009: Metrics of hurricane–ocean interaction: Vertically-integrated or vertically-averaged ocean temperature? *Ocean Sci.*, **5**, 351–368, doi:10.5194/os-5-351-2009.

Puy, M., J. Vialard, M. Lengaigne, and E. Guilyardi, 2016: Modulation of equatorial Pacific westerly/easterly wind events by the Madden–Julian oscillation and convectively-coupled Rossby waves. *Climate Dyn.*, **46**, 2155–2178, doi:10.1007/s00382-015-2695-x.

Radon, J., 1917: Über dies Bestimmung von Funktionen durch ihre integralwerte längs gewisser Mannigfaltigkeiten. *Ber. Verh. Sächs. Akad. Wiss.*, **69**, 262–267.

Raga, G. B., and Coauthors, 2013: Landfalling tropical cyclones on the Pacific coast of Mexico: 1850–2010. *Atmósfera*, **26** (2), 209–220, doi:10.1016/S0187-6236(13)71072-5.

Rasmusson, E. M., and T. H. Carpenter, 1982: Variations in tropical sea surface temperature and surface wind fields associated with the Southern Oscillation/El Niño. *Mon. Wea. Rev.*, **110**, 354–384, doi:10.1175/1520-0493(1982)110<0354:VITSST>2.0.CO;2.

Ren, H.-L., and F.-F. Jin, 2013: Recharge oscillator mechanisms in two types of ENSO. *J. Climate*, **26**, 6506–6523, doi:10.1175/JCLI-D-12-00601.1.

Ritchie, E. A., K. M. Wood, D. S. Gutzler, and S. R. White, 2011: The influence of eastern Pacific tropical cyclone remnants on the southwestern United States. *Mon. Wea. Rev.*, **139**, 192–210, doi:10.1175/2010MWR3389.1.

Roundy, P. E., and G. N. Kiladis, 2006: Observed relationship between oceanic Kelvin waves and atmospheric forcing. *J. Climate*, **19**, 5253–5272, doi:10.1175/JCLI3893.1.

Saha, S., and Coauthors, 2006: The NCEP Climate Forecast System. *J. Climate*, **19**, 3483–3517, doi:10.1175/JCLI3812.1.

Shay, L. K., and J. K. Brewster, 2010: Oceanic heat content variability in the eastern Pacific Ocean for hurricane intensity forecasting. *Mon. Wea. Rev.*, **138**, 2110–2131, doi:10.1175/2010MWR3189.1.

Sobel, A. H., S. J. Camargo, A. G. Barnston, and M. K. Tippett, 2016: Northern Hemisphere tropical cyclones during the quasi–El Niño of late 2014. *Nat. Hazards*, **83**, 1717–1729, doi:10.1007/s11069-016-2389-7.

Spillane, M. C., D. B. Enfield, and J. S. Allen, 1987: Intraseasonal oscillations in sea level along the west coast of the Americas. *J. Phys. Oceanogr.*, **17**, 313–325, doi:10.1175/1520-0485(1987)017<0313:IOISLA>2.0.CO;2.

Sprintall, J., A. L. Gordon, R. Murtugudde, and R. D. Susanto, 2000: A semiannual Indian Ocean forced Kelvin wave observed in the Indonesian Seas in May 1997. *J. Geophys. Res.*, **105**, 17 217–17 230, doi:10.1029/2000JC900065.

Stein, K., A. Timmermann, and N. Schneider, 2011: Phase synchronization of the El Niño–Southern Oscillation with the annual cycle. *Phys. Rev. Lett.*, **107**, 128501, doi:10.1103/PhysRevLett.107.128501.

Suarez, M. J., and P. S. Schopf, 1988: A delayed action oscillator for ENSO. *J. Atmos. Sci.*, **45**, 3283–3287, doi:10.1175/1520-0469(1988)045<3283:ADAOFE>2.0.CO;2.

Takahashi, K., A. Montecinos, K. Goubanova, and B. Dewitte, 2011: ENSO regimes: Reinterpreting the canonical and Modoki El Niño. *Geophys. Res. Lett.*, **38**, L10704, doi:10.1029/2011GL047364.

Torrence, C., and G. P. Compo, 1998: A practical guide to wavelet analysis. *Bull. Amer. Meteor. Soc.*, **79**, 61–78, doi:10.1175/1520-0477(1998)079<0061:APGTWA>2.0.CO;2.

Vincent, E. M., K. A. Emanuel, M. Lengaigne, J. Vialard, and G. Madec, 2014: Influence of upper-ocean stratification interannual variability on tropical cyclones. *J. Adv. Model. Earth Syst.*, **6**, 680–699, doi:10.1002/2014MS000327.

Vitart, F., 2009: Impact of the Madden Julian oscillation on tropical storms and risk of landfall in the ECMWF forecast system. *Geophys. Res. Lett.*, **36**, L15802, doi:10.1029/2009GL039089.

Waliser, D. E., 2006: Predictability of tropical intraseasonal variability. *Predictability of Weather and Climate*, T. Palmer and R. Hagedorn, Eds., Cambridge University Press, 275–365.

Wang, B., 2003: Kelvin waves. *Encyclopedia of Meteorology*. J. Holton, Ed., Academic Press, 1062–1067.

Wang, C., and S.-K. Lee, 2009: Co-variability of tropical cyclones in the North Atlantic and the eastern North Pacific. *Geophys. Res. Lett.*, **36**, L24702, doi:10.1029/2009GL041469.

Wood, K. M., and E. A. Ritchie, 2013: An updated climatology of tropical cyclone impacts on the southwestern United States. *Mon. Wea. Rev.*, **141**, 4322–4336, doi:10.1175/MWR-D-13-00078.1.

Yuan, D., 2005: Role of the Kelvin and Rossby waves in the seasonal cycle of the equatorial Pacific Ocean circulation. *J. Geophys. Res.*, **110**, C04004, doi:10.1029/2004JC002344.

Zhai, F., and D. Hu, 2013: Revisit the interannual variability of the North Equatorial Current transport with ECMWF ORA-S3. *J. Geophys. Res. Oceans*, **118**, 1349–1366, doi:10.1002/jgrc.20093.